

# Exciton-assisted low-energy magnetic excitations in a photoexcited Mott insulator on the square lattice

Kenji Tsutsui,<sup>1,\*</sup> Kazuya Shinjo,<sup>2</sup> Shigetoshi Sota,<sup>3</sup> and Takami Tohyama<sup>4,†</sup>

<sup>1</sup>*Synchrotron Radiation Research Center, National Institutes for Quantum Science and Technology, Hyogo 679-5148, Japan*

<sup>2</sup>*Computational Quantum Matter Research Team,*

*RIKEN Center for Emergent Matter Science (CEMS), Wako, Saitama 351-0198, Japan*

<sup>3</sup>*Computational Materials Science Research Team,*

*RIKEN Center for Computational Science (R-CCS), Kobe, Hyogo 650-0047, Japan*

<sup>4</sup>*Department of Applied Physics, Tokyo University of Science, Tokyo 125-8585, Japan*

(Dated: July 7, 2022)

Photoexcitation of a Mott insulator on a square lattice has weakened the intensity of both single- and two-magnon as observed in time-resolved resonant-inelastic x-ray scattering and time-resolved Raman scattering. However, the spectral change in low-energy regions below the magnons has not been clarified so far. To uncover the nature of photoinduced low-energy magnetic excitations of the Mott insulator, we numerically investigate transient magnetic dynamics in a photoexcited half-filled Hubbard model on the square lattice. After turning off a pump pulse tuned for an absorption edge, new magnetic signals clearly emerge well below magnon energy in both single- and two-magnon excitations. We find that the low-energy excitations are predominantly created via excitonic states at the absorption edge. These exciton-assisted magnetic excitations may provide a possible explanation for low-energy spectral weight in a recent time-resolved two-magnon Raman scattering experiment for insulating  $\text{YBa}_2\text{Cu}_3\text{O}_{6.1}$ .

## I. INTRODUCTION

Photoirradiation to Mott insulators on a square lattice induces drastic changes of electronic states such as a photoinduced insulator-to-metal transition [1–3]. The suppression of absorption spectral weights across the Mott gap and the emergence of low-energy charge excitations inside the Mott gap in the optical conductivity are indications of the photoinduced insulator-to-metal transition. Not only the charge channel but also spin channel may produce characteristic changes. The optical-pump, terahertz-probe spectroscopy and femtosecond stimulated Raman scattering have reported spin dynamics in insulating antiferromagnet  $\text{TbMnO}_3$  [4] and  $\text{KNiF}_3$  [5], respectively. In antiferromagnetic Mott insulators, the decrease of spectral weights on single-magnon dispersion due to photoirradiation has been observed in time-resolved resonant-inelastic x-ray scattering (trRIXS) for  $\text{Sr}_2\text{IrO}_4$  [6] and  $\text{Sr}_3\text{Ir}_2\text{O}_7$  [7], where RIXS can detect spin-flip excitations when incident x rays are tuned for  $L$  edge in transition metals [8]. Time-resolved two-magnon Raman scattering (trTMR) for an antiferromagnetic Mott insulator  $\text{YBa}_2\text{Cu}_3\text{O}_{6.1}$  [2] has also reported the decrease of two-magnon weights. These decreases are naturally understood as a result of the emergence of photoexcited electronic states that reduces antiferromagnetic spin correlation as proposed theoretically [10, 11].

An arising question is whether low-energy magnetic excitations below magnons emerge or not in the spin channel. In fact, the trTMR experiment has reported

an increase of low-energy spectral weight below the two-magnon energy around  $1000\text{ cm}^{-1}$  to  $1500\text{ cm}^{-1}$  for photoirradiated  $\text{YBa}_2\text{Cu}_3\text{O}_{6.1}$  [2]. A possible interpretation of the weight would be just a shift of weight from a two-magnon peak due to broadening of the peak. Since photoirradiation to Mott insulators changes electronic states drastically as seen in the charge channel, it is natural to expect that the spin channel will also induce low-energy excitations below magnon energies.

In this Communication, we theoretically propose photoinduced low-energy magnetic excitations below single- and two-magnon energies in a photoexcited Mott insulator on a square lattice. Using a numerically exact-diagonalization (ED) technique and time-dependent density-matrix renormalization group (tDMRG) for a photoexcited half-filled Hubbard model on the square lattice, we find low-energy magnetic excitations induced by a pump pulse, whose intensity is maximized when the frequency of the pulse is tuned for absorption edge. Analyzing the low-energy magnetic excitation by using point-group symmetry for the square lattice, we clarify that the photoinduced low-energy signals are predominantly created via photoexcited states with the  $E$  presentation of the  $C_{4v}$  point group, which are excitonic states at the absorption edge [12]. The proposed exciton-assisted photoinduced magnetic excitations will give one of possible origins for low-energy weight in the trTMR spectrum. This theoretical prediction will be confirmed if pumping frequency is varied in the trTMR experiment.

\* [tsutsui.kenji@qst.go.jp](mailto:tsutsui.kenji@qst.go.jp)

† [tohyama@rs.tus.ac.jp](mailto:tohyama@rs.tus.ac.jp)

## II. RESULTS

### A. Model

In order to describe Mott insulating states on a square lattice, we take a single-band Hubbard model at half filling given by

$$H_0 = -t_h \sum_{i\delta\sigma} c_{i\sigma}^\dagger c_{i+\delta\sigma} + U \sum_i n_{i\uparrow} n_{i\downarrow}, \quad (1)$$

where  $c_{i\sigma}^\dagger$  is the creation operator of an electron with spin  $\sigma$  at site  $i$ , number operator  $n_{i\sigma} = c_{i\sigma}^\dagger c_{i\sigma}$ ,  $i + \delta$  represents four nearest-neighbor sites around site  $i$ .  $t_h$  and  $U$  are the nearest-neighbor hopping and on-site Coulomb interaction, respectively. We take  $U/t_h = 10$ , which guarantees antiferromagnetic Mott insulating ground state at half filling. Note that  $t_h \sim 0.35$  eV for cuprates.

We incorporate an external electric field via the Peierls substitution in the hopping term,  $c_{i,\sigma}^\dagger c_{i+\delta,\sigma} \rightarrow e^{i\mathbf{A}(t)\cdot\mathbf{R}_\delta} c_{i,\sigma}^\dagger c_{i+\delta,\sigma}$ , leading to a time-dependent driven Hamiltonian  $H(t)$ . Here,  $\mathbf{R}_\delta$  is the vector from  $i$  to  $i + \delta$ , and  $\mathbf{A}(t)$  is the vector potential given by  $\mathbf{A}(t) = \mathbf{A}_0 e^{-(t-t_0)^2/(2t_d^2)} \cos[\omega_p(t-t_0)]$ , where a Gaussian-like envelope centered at  $t_0$  has a temporal width  $t_d$  and a central frequency  $\omega_p$ . We apply an external electric field along the  $x$  direction without being otherwise specified, i.e.,  $\mathbf{A}_0 = (A_0, 0)$ , and set  $A_0 = 0.5$ ,  $t_0 = 0$ , and  $t_d = 0.5$ . Hereafter we use  $t_h = 1$  as an energy unit and  $1/t_h$  as a time unit.

In calculating time-resolved spin excitation in trRIXS during pumping, a real-time representation of cross section has been used for a Hubbard model on a square lattice [13, 14]. Instead, we focus on time-resolved spin excitation after pumping. In such a case, it is convenient to use time-dependent wave function  $|\psi(t)\rangle$  as an initial state of a two-particle correlation function for a time region after turning off the pump pulse,  $t > t_{\text{off}}$ , where the Hamiltonian is time-independent. Applying this procedure, we obtain time-resolved dynamical correlation function with momentum  $\mathbf{q}$  and frequency  $\omega$  for a  $\mathbf{q}$ -dependent physical quantity  $O_{\mathbf{q}}$  as [15]

$$\begin{aligned} O(\mathbf{q}, \omega; t) &= \frac{1}{\pi} \text{Re} \int_t^\infty ds e^{i(\omega+i\eta)s} \langle \psi(t) | [O_{\mathbf{q}}(s), O_{-\mathbf{q}}] | \psi(t) \rangle \quad (2) \\ &= -\frac{1}{\pi} \text{Im} \sum_{m,n} \frac{1}{\omega - (\varepsilon_n - \varepsilon_m) + i\eta} \\ &\quad \times [\langle \psi(t) | m \rangle \langle m | O_{\mathbf{q}} | n \rangle \langle n | O_{-\mathbf{q}} | \psi(t) \rangle \\ &\quad - \langle \psi(t) | O_{-\mathbf{q}} | m \rangle \langle m | O_{\mathbf{q}} | n \rangle \langle n | \psi(t) \rangle], \quad (3) \end{aligned}$$

where the operator  $O_{\mathbf{q}}(s) = e^{iH_0 s} O_{\mathbf{q}} e^{-iH_0 s}$ ,  $H_0 |m\rangle = \varepsilon_m |m\rangle$ ,  $\eta$  is a small positive number, and  $|\psi(t)\rangle = e^{-iH_0(t-t_{\text{off}})} |\psi(t_{\text{off}})\rangle$ . We note that replacing  $|\psi(t)\rangle$  by the ground state  $|0\rangle = |\psi(-\infty)\rangle$  in Eq. (2) formally gives the equilibrium dynamical correlation function  $O(\mathbf{q}, \omega)$ . For a  $L$ -site periodic lattice, we choose

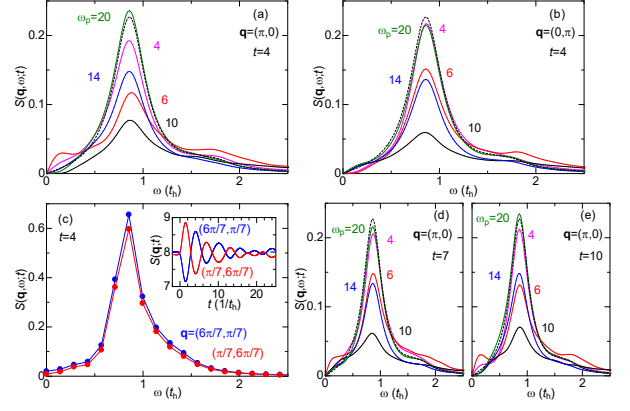


FIG. 1. **Pumping frequency  $\omega_p$  dependence of time-resolved dynamical spin correlation function  $S(\mathbf{q}, \omega; t)$  after pumping.** A half-filled Hubbard model on square lattices with  $U = 10$  is used. (a)  $\mathbf{q} = (\pi, 0)$  and (b)  $\mathbf{q} = (0, \pi)$  for a periodic  $4 \times 4$  lattice obtained by ED at  $t = 4$ . (c)  $\omega_p = 20$  and  $t = 4$  for  $\mathbf{q} = (\pi/7, 6\pi/7)$  (red circles) and  $\mathbf{q} = (6\pi/7, \pi/7)$  (blue circles) in a  $6 \times 6$  lattice with open boundary conditions obtained by tDMRG. Inset shows time-resolved static spin structure factor  $S(\mathbf{q}; t)$ . An antiphase oscillation appears similar to the previous result by ED [1]. (d)  $t = 7$  and (e)  $t = 10$  at  $\mathbf{q} = (\pi, 0)$  for the  $4 \times 4$  lattice by ED. In (a), (b), (d), and (e), dashed black lines represent the results before pumping, while purple, red, black, blue, and green solid lines represent the results at  $\omega_p = 4, 6, 10, 14,$  and  $20$ , respectively.

$O_{\mathbf{q}} = S_{\mathbf{q}}^z = L^{-1/2} \sum_i e^{-i\mathbf{q}\cdot\mathbf{R}_i} S_i^z$  for the time-resolved dynamical spin correlation function  $S(\mathbf{q}, \omega; t)$  and  $O_{\mathbf{q}} = \sum_{\mathbf{k}} (\cos k_x - \cos k_y) \mathbf{S}_{\mathbf{k}+\mathbf{q}} \cdot \mathbf{S}_{-\mathbf{k}}$  with  $\mathbf{q} = 0$  for trTMR spectrum  $M(\omega; t)$  with  $B_{1g}$  representation, where  $S_i^z$  is the  $z$  component of a spin operator  $\mathbf{S}_i$  at site  $i$ . The first term in Eq. (3), denoted hereafter as  $O_1(\mathbf{q}, \omega; t)$ , is related to the second term,  $O_2(\mathbf{q}, \omega; t)$ , with the form  $O_2(\mathbf{q}, \omega; t) = -O_1(\mathbf{q}, -\omega; t)$ , being  $O(\mathbf{q}, \omega; t) = O_1(\mathbf{q}, \omega; t) + O_2(\mathbf{q}, \omega; t) = O_1(\mathbf{q}, \omega; t) - O_1(\mathbf{q}, -\omega; t)$ . We note that the integration of  $S_1(\mathbf{q}, \omega; t)$  with respect to  $\omega$  ( $-\infty \leq \omega \leq \infty$ ) gives the time-resolved static spin structure factor  $S(\mathbf{q}; t) \equiv \langle \psi(t) | S_{\mathbf{q}}^z S_{-\mathbf{q}}^z | \psi(t) \rangle$ . The time-dependent wave function  $|\psi(t)\rangle$  is given by procedures mentioned in Sec. IV.

### B. Low-energy excitation below single magnon

We first show the results of  $S(\mathbf{q}, \omega; t)$ , which can describe photoinduced low-energy magnetic excitations located below single-magnon dispersion. For a  $4 \times 4$  lattice, we take  $\mathbf{q} = (\pi, 0)$  and  $(0, \pi)$ , where the energy of single magnon becomes maximum. Figures 7(a) and 7(b) show the pumping frequency  $\omega_p$  dependence of  $S(\mathbf{q}, \omega; t)$  at  $\mathbf{q} = (\pi, 0)$  and  $(0, \pi)$ , respectively, for  $t = 4$ . A peak at  $\omega = 0.8$  represents a single-magnon excitation at a given  $\mathbf{q}$ . At high pumping frequency  $\omega_p = 20 > U$ , the peak intensity is larger and smaller than that before pumping

(dotted lines) in Figs. 7(a) and 7(b), respectively. This  $\mathbf{q}$ -dependent intensity at a given  $t$  is a consequence of an antiphase oscillation of time-dependent spin structure factors in a photoexcited Mott insulator on the square lattice proposed by the present authors [1] [see also the inset of Fig. 7(c)]. With decreasing  $\omega_p$ , the peak intensity decreases and shows a minimum at  $\omega_p = 10$ , where absorbed energy by pumping in the system is largest, leading to the weakening of antiferromagnetic spin correlation [13, 14]. With further decreasing  $\omega_p$ , the peak intensity increases.

At  $\omega_p = 6$  that agrees with an absorption-peak energy at the Mott-gap edge [17], we find a hump structure at  $\omega = 0.2$  below the peak energy for  $\mathbf{q} = (\pi, 0)$ . This is indeed a photoinduced low-energy magnetic excitation. It is interesting that away from  $\omega_p = 6$  the hump structure loses its weight. In particular, when  $\omega_p$  satisfies off-resonance condition, i.e.,  $\omega_p = 20$ , the hump structure is hardly identified. This behavior may not be system-size dependent. To confirm this, we perform tDMRG calculations of  $S(\mathbf{q}, \omega; t)$  for a  $6 \times 6$  lattice with open boundary conditions (see Sec. IV) and show  $S(\mathbf{q}, \omega; t = 4)$  at  $\mathbf{q} = (6\pi/7, \pi/7)$  and  $\mathbf{q} = (\pi/7, 6\pi/7)$  for  $\omega_p = 20$  in Fig. 7(c). Since the time-resolved static spin structure factor  $S(\mathbf{q}; t = 4)$  shows a value larger at  $\mathbf{q} = (\pi/7, 6\pi/7)$  than at  $\mathbf{q} = (6\pi/7, \pi/7)$  as shown in the inset of Fig. 7(c), the magnon peak at  $\omega = 0.6$  is larger in intensity at  $\mathbf{q} = (\pi/7, 6\pi/7)$  than at  $\mathbf{q} = (6\pi/7, \pi/7)$ . However, we find no clear hump at low-energy region in both  $\mathbf{q}$ s, which is the same as the results at  $\omega_p = 20$  for the  $4 \times 4$  periodic lattice. This indicates that the effects of system size and boundary conditions are small.

It is interesting to notice that there is no hump structure at  $\mathbf{q} = (0, \pi)$  in Fig. 7(b) for  $\omega_p = 6$ . Since the pump pulse is polarized along the  $x$  direction, it would be reasonable to find the difference of low-energy magnetic excitations between  $\mathbf{q} = (\pi, 0)$  and  $(0, \pi)$ . We will discuss this in Sec. III.

The  $\omega_p$  dependence of the low-energy hump structure at  $\mathbf{q} = (\pi, 0)$  is unchanged when  $t = 7$  and  $t = 10$  as shown in Figs. 7(d) and 7(e), respectively. This means that the hump intensity does not oscillate with time in contrast to the peak intensity [1]. Therefore, it would be possible to detect this hump in trRIXS for insulating cuprates and iridates on square lattices when a pump pulse tuned for a Mott-gap edge is applied along the  $x$  direction and momentum transfer is set to  $\mathbf{q} = (\pi, 0)$ .

In order to understand the origin of the hump structure at  $\omega_p = 6$ , we decompose  $S(\mathbf{q}, \omega; t)$  at  $\mathbf{q} = (\pi, 0)$  and  $t = 4$  into several contributions by taking into account the fact that  $|\psi(t)\rangle$  for  $t > t_{\text{off}}$  has three components made from irreducible representations,  $A_1$ ,  $E$ , and  $B_1$ , of the square lattice with the  $C_{4v}$  point group:

$$|\psi(t)\rangle = |\psi_{A_1}(t)\rangle + |\psi_E(t)\rangle + |\psi_{B_1}(t)\rangle. \quad (4)$$

The first, second, and third terms come predominantly from the ground state, single-photon absorbed states, and two-photon absorbed states including  $B_{1g}$  Raman

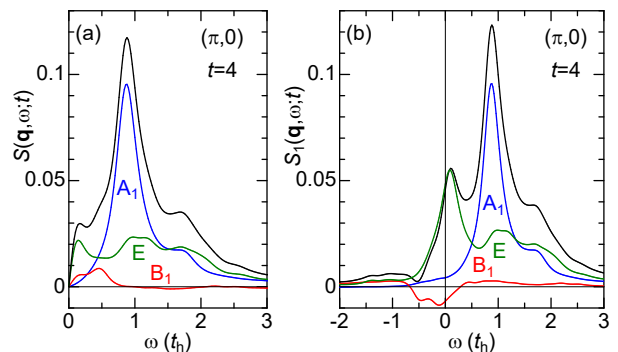


FIG. 2. **Symmetry decomposition of the time-resolved dynamical spin correlation functions.**  $\mathbf{q} = (\pi, 0)$  and  $t = 4$  in the case of  $\omega_p = 6$  for a half-filled  $4 \times 4$  periodic Hubbard lattice with  $U = 10$ . (a)  $S(\mathbf{q}, \omega; t)$  and (b)  $S_1(\mathbf{q}, \omega; t)$ . Note that  $S(\mathbf{q}, \omega; t) = S_1(\mathbf{q}, \omega; t) - S_1(\mathbf{q}, -\omega; t)$ . Black solid lines are the total sum of each contribution (blue, green, and red solid lines for  $A_1$ ,  $E$ , and  $B_1$  of the  $C_{4v}$  point group, respectively).

active state, respectively. Figure 8(a) exhibits the three contributions to the  $S(\mathbf{q} = (\pi, 0), \omega; t = 4)$ , where the  $A_1$ ,  $E$ , and  $B_1$  states in Eq. (4) couple to final states with  $A_1$ ,  $B_1$ , and  $A_1$ , respectively, at  $\mathbf{q} = (\pi, 0)$ . We find that the magnon peak consists mainly of the  $A_1$  state in Eq. (4). This makes sense because of the presence of significant ground-state contribution in the  $A_1$  state. On the other hand, we find that the  $E$  state has the largest contribution around  $\omega = 0.2$ .

Since  $S(\mathbf{q}, \omega; t)$  in Eq. (3) has two contributions, i.e., one from the first term denoted by  $S_1(\mathbf{q}, \omega; t)$  and the other from the second term  $S_2(\mathbf{q}, \omega; t)$ , it is crucial to identify which term is dominating low-energy excitations. In Fig. 8(b), we show  $S_1(\mathbf{q}, \omega; t)$  at  $\mathbf{q} = (\pi, 0)$  decomposed by irreducible representations as in Fig. 8(a). We note that  $S(\mathbf{q}, \omega; t) = S_1(\mathbf{q}, \omega; t) - S_1(\mathbf{q}, -\omega; t)$  for  $\omega \geq 0$ . This is indeed the reason why the spectral weight at  $\omega = 0$  is exactly zero in  $S(\mathbf{q}, \omega; t)$ . We find that the  $E$  component in  $S_1(\mathbf{q}, \omega; t)$  has large weight at  $\omega = 0.1$ . This weight results in the  $\omega = 0.2$  hump structure in  $S(\mathbf{q}, \omega; t)$ . Such a large weight near  $\omega = 0$  in  $S_1(\mathbf{q}, \omega; t)$  implies the presence of very low-energy magnetic excitations from the single-photon absorbed  $E$  state at the Mott-gap edge as will be discussed in Sec. III.

### C. Low-energy excitation below two magnons

Photoirradiation may induce low-energy magnetic excitations below two-magnon energy. To confirm this, we perform ED calculations of trTMR spectrum after turning off the pump pulse using the  $4 \times 4$  periodic half-filled Hubbard lattice. Figure 3 shows the  $\omega_p$  dependence of  $M(\omega; t)$  at  $t = 4$ . The pump pulse suppresses the intensity of a two-magnon peak at  $\omega = 1$ , which has been observed in the trTMR experiment for photoirradiated

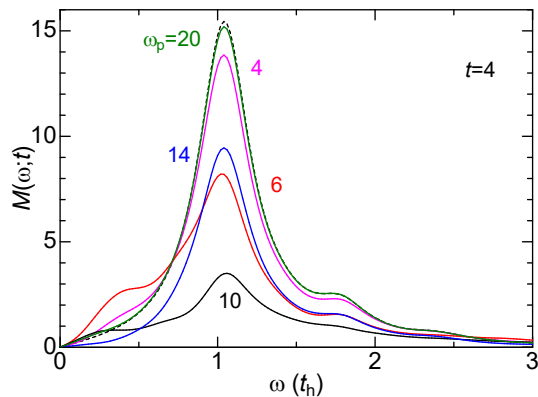


FIG. 3. **Pumping frequency  $\omega_p$  dependence of trTMR spectra  $M(\omega; t)$  after pumping.**  $t = 4$  for a half-filled  $4 \times 4$  Hubbard lattice with  $U = 10$ . Dashed black line represents the results before pumping, while purple, red, black, blue, and green solid lines represent the results at  $\omega_p = 4, 6, 10, 14,$  and  $20$ , respectively.

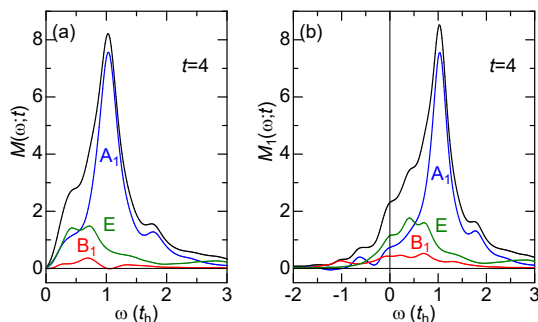


FIG. 4. **Symmetry decomposition of trTMR spectra.**  $t = 4$  in the case of  $\omega_p = 6$  for a half-filled  $4 \times 4$  periodic Hubbard lattice with  $U = 10$ . (a)  $M(\omega; t)$  and (b)  $M_1(\omega; t)$ . Note that  $M(\omega; t) = M_1(\omega; t) - M_1(-\omega; t)$ . Black solid lines are the total sum of each contribution (blue, green, and red solid lines for  $A_1, E,$  and  $B_1$  of the  $C_{4v}$  point group, respectively).

$\text{YBa}_2\text{Cu}_3\text{O}_{6.1}$  [2]. The peak-intensity variation with respect to  $\omega_p$  is similar to single-magnon intensity shown in Figs. 8(a) and 8(b).

When  $\omega_p = 6$ , we find an enhancement of low-energy spectral weight around  $\omega = 0.4$ . This is similar to the enhancement of low-energy weight in  $S(\mathbf{q}, \omega; t)$  shown in Fig. 8(a), though its energy in  $S(\mathbf{q}, \omega; t)$  is nearly a half of  $\omega = 0.4$ . This similarity suggests same origin of these enhancements. To clarify what symmetry components contribute to the enhancement in trTMR, we decompose the spectral weight into several components characterized by irreducible representations as is the case of Fig. 8. We show them in Fig. 4. Similar to  $S(\mathbf{q}, \omega; t)$ , the low-energy part of  $M(\omega; t)$  comes from the E component as shown in Fig. 4(a). From Fig. 4(b), this E component is found to be originated from the first term in Eq.(3),  $M_1(\omega; t)$ . In other words, the low-energy excitation around  $\omega = 0.4$  in  $M(\omega; t)$  is a consequence of magnetic excitations from

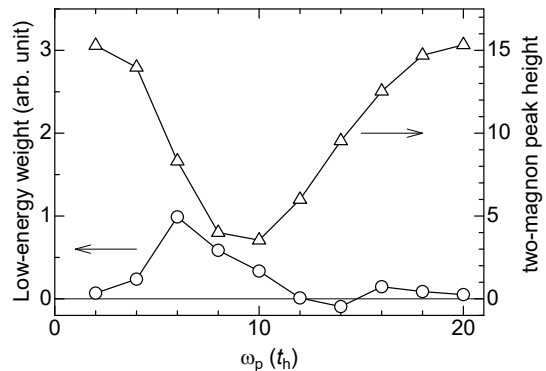


FIG. 5. **Pumping frequency  $\omega_p$  dependence of trTMR spectrum.** Low-energy spectral weight below  $\omega = 0.7$  (open squares) and height of two-magnon peak (open triangles) obtained from  $M(\omega; t = 4)$  shown in Fig. 3.

a single-photon absorbed state at the Mot-gap edge.

In order to investigate the  $\omega_p$  dependence of trTMR in more detail, we analyze low-energy spectral weight below  $\omega = 0.7$  in  $M(\omega; t = 4)$  shown in Fig. 3. The weight is evaluated by subtracting the contribution of two-magnon peak that is fitted by a single Lorentzian. Figure 5 shows the low-energy weight together with the two-magnon peak height as a function of  $\omega_p$ . The peak height decreases with increasing  $\omega_p$  and exhibits a minimum at  $\omega_p = 10$  corresponding to the center of optical absorption spectrum for  $U = 10$  [17]. On the contrary, the low-energy weight exhibits a maximum at  $\omega_p = 6$  corresponding to the Mott-gap edge. The difference of  $\omega_p$  showing the peak-height minimum and low-energy weight maximum clearly demonstrates that the enhancement of low-energy excitation is not due to spectral weight transfer from the two-magnon peak. Based on this result, we can predict different  $\omega_p$  dependence between the low-energy weight and peak height in trTMR for Mott insulators on the square lattice such as  $\text{YBa}_2\text{Cu}_3\text{O}_{6.1}$ .

### III. DISCUSSIONS

In Sec. II, we have found that low-energy magnetic excitations in both  $S(\mathbf{q}, \omega; t)$  and  $M(\omega; t)$  are induced when a pumping frequency  $\omega_p$  is tuned for the Mott-gap edge at  $\omega = 6$  [17]. We have also found that the state with the E representation in  $|\psi(t)\rangle$  significantly contributes to the low-energy magnetic excitations as shown in Figs. 8 and 4. Since there is an excitonic peak at the Mott-gap edge in the optical conductivity [12, 17], which comes from a dipole-allowed state with the E representation, it is reasonable to suppose that the low-energy magnetic excitations are related to the excitonic state. In fact, we separately confirmed that the E component of  $S_1(\mathbf{q} = (\pi, 0), \omega; t = 4)$  in Fig. 8(b) [ $M_1(\omega; t = 4)$  in Fig. 3(b)] is almost equivalent to the equilibrium  $S(\mathbf{q} = (\pi, 0), \omega)$  [ $M(\omega)$ ] obtained by regard-

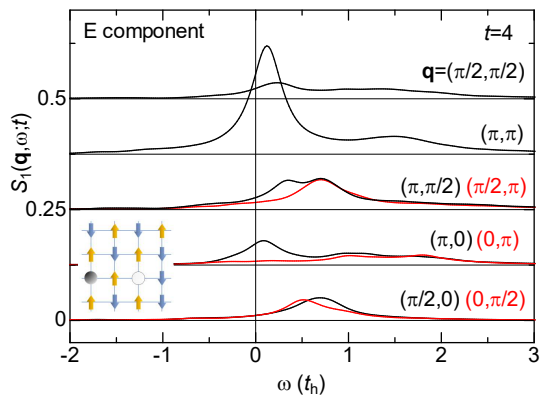


FIG. 6.  $\mathbf{q}$  dependence of symmetry-decomposed  $E$  component of  $S_1(\mathbf{q}, \omega; t)$ .  $t = 4$  in the case of  $\omega_p = 6$  for a half-filled  $4 \times 4$  periodic Hubbard lattice with  $U = 10$ . The results at  $\mathbf{q} = (\pi, 0)$  is the same as that in Fig. 8(b). The inset shows a configuration with the largest weight in a  $E$ -symmetry excitonic state at the Mott-gap edge that contributes to  $|\psi_E(t)\rangle$  in Eq. (4). The white (black) circle represents a holon (doublon) surrounded by up and down spins that arrange antiferromagnetically along the  $x$  direction but less antiferromagnetic correlation along the  $y$  direction.

ing the excitonic state as an initial state. This is strong evidence that the photoinduced magnetic excitations are assisted by the excitonic state.

We notice that the  $E$  component below the main peak of  $M_1(\omega; t = 4)$  in Fig. 4(b) is wider in energy than that of  $S_1(\mathbf{q} = (\pi, 0), \omega; t = 4)$  in Fig. 8(b). The wide distribution in  $M_1(\omega; t)$  can be understood by taking into account the fact that two-magnon excitations are a combination of a pair of single magnons with opposite momenta. That is,  $M_1(\omega; t)$  is composed of a sum of  $S_1(\mathbf{q}, \omega; t)$  with different momenta. To elucidate this wide distribution of the  $E$  component in  $M_1(\omega; t = 4)$  for  $\omega_p = 6$ , it is instructive to calculate the  $E$  component of  $S_1(\mathbf{q}, \omega; t = 4)$  for all of  $\mathbf{q}$ . We show the  $\mathbf{q}$  dependence in Fig. 5. Note that the result for  $\mathbf{q} = (\pi, 0)$  is already shown in Fig. 8(b). We find that the  $\mathbf{q} = (\pi, 0)$  excitation as well as the  $(\pi, \pi)$  one is the lowest in energy while other  $\mathbf{q}$ s have higher excitation energy. Since many pairs of single magnons with higher energy, such as a pair at  $\mathbf{q} = (\pm\pi/2, 0)$ , contributes to  $M_1(\omega; t)$ , the distribution of the  $E$  component in  $M_1(\omega; t = 4)$  becomes wider. At the same time, Figure 5 explains the fact that photoinduced magnetic excitations in  $S(\mathbf{q} = (\pi, 0), \omega; t = 4)$  are lower in energy than that of  $M(\omega; t = 4)$ .

We finally comment on why the  $\mathbf{q} = (\pi, 0)$  excitation is lowest in energy in Fig. 5. This may come from magnetic configurations in the excitonic state. In this state, there is a holon-doublon pair surrounded by localized spins in the background. The pair is created along the  $x$  direction parallel to an applied electric field as evidenced in the inset of Fig. 5, which shows a dominant configuration in the excitonic state. We find that the spins arrange antiferromagnetically along the  $x$  direction, while they have less

antiferromagnetic correlation along the  $y$  direction. This may lead to spin arrangement with momentum  $\mathbf{q} = (\pi, 0)$  in the excitonic state. This view is consistent with a separate numerical simulation of spin and charge correlation in the excitonic state [18], which also reports anisotropic correlation between the  $x$  and  $y$  directions.

Recent trTMR experiment has reported an increase of low-energy spectral weight around 0.15 eV ( $1000 \text{ cm}^{-1}$  to  $1500 \text{ cm}^{-1}$ ) for  $\text{YBa}_2\text{Cu}_3\text{O}_{6.1}$  [2] when the material is driven by 1.5 eV pump pulse. Our finding that low-energy magnetic excitations below the two-magnon peak emerge when the Mott-gap edge region is driven by pump pulse is consistent with the experimental observation. In the trTMR experiment, the polarization of pump photon was the (1,1) direction, which is different from our (1,0) direction. We confirmed that even for the (1,1) direction, low-energy excitations emerge in our calculation (see Supplementary Note). In real cuprates, the second-neighbor hopping  $t'_h$  may not be neglected. We also confirmed that the presence of  $t'_h (= -0.25)$  does not change the emergence of low-energy magnetic excitations in trTMR (see also Supplementary Note). To confirm our finding, we propose trTMR experiments changing the pumping frequency, where the low-energy weight is expected to be maximum for the 1.5 eV pump pulse.

In summary, we have theoretically proposed photoinduced low-energy magnetic excitations below single- and two-magnon energies in a driven Mott insulator on a square lattice. The intensity of the low-energy magnetic excitations is maximized when the frequency of the pulse is tuned for absorption edge and optically allowed states with the  $E$  presentation of the  $C_{4v}$  point group are excited. The excitations are thus assisted by excitonic states at the Mott-gap edge. The proposed photoinduced low-energy magnetic excitations agree with the increase of low-energy weight in the trTMR spectrum previously reported [2]. This theoretical prediction will be confirmed if pumping frequency is varied in the trTMR experiment as well as trRIXS experiment for insulating cuprates and iridates.

#### IV. METHODS

We use a square-lattice periodic Hubbard cluster with  $L = 4 \times 4$  to calculate the time-resolved dynamical spin correlation function and time-resolved two-magnon Raman spectrum by the Lanczos-type exact diagonalization method. Time-dependent wave function is given by  $|\psi(t + \Delta t)\rangle = e^{-iH(t)\Delta t}|\psi(t)\rangle$  with a time step  $\Delta t$ . Using a Taylor expansion [19], we obtain  $|\psi(t + \Delta t)\rangle = \sum_{n=0}^{\infty} |\varphi_n(t)\rangle$  with  $|\varphi_n(t)\rangle = (-iH(t)\Delta t)^n/n!|\psi(t)\rangle$ . Each term is iteratively obtained by  $|\varphi_{n+1}(t)\rangle = -iH(t)\Delta t/(n+1)|\varphi_n(t)\rangle$  starting from  $|\varphi_0\rangle = |\psi(t)\rangle$ . We use  $\Delta t = 0.01$  and the summation with respect to  $n$  is truncated if the norm  $\langle \varphi_n(t)|\varphi_n(t)\rangle$  is smaller than a critical value such as  $10^{-14}$ . For time-dependent dynamical quantities, we use Eq. (3) with

$\eta = 0.2$ , where we perform continuum-fraction expansions based on the Lanczos method starting from two initial states  $|\psi(t)\rangle$  and  $O_{-q}|\psi(t)\rangle$ .

We also use a  $L = 6 \times 6$  lattice with open boundary conditions for the calculation of the time-resolved dynamical spin correlation function by tDMRG. Expanding time-evolution operator using the spherical Bessel function  $j_l(x)$  of the first kind and the Legendre polynomial  $P_l(x)$  up to  $M$ -th order as  $e^{-iH(t)\Delta t} \simeq C(t) \sum_{l=0}^M (-1)^l (2l+1) j_l(\delta t/\omega_s(t)) P_l(H_s(t))$ , where a scaled Hamiltonian  $H_s(t) = \omega_s(t)[H(t) - \lambda_s(t)]$  with scaling parameters  $\omega_s(t)$  and  $\lambda_s(t)$  and  $C(t)$  is a normalization factor, we use two target states,  $|\psi(t)\rangle$  and  $|\psi(t + \Delta t)\rangle$ , in the DMRG procedure for a given  $t$ , in order to construct a basis set that can express wave functions in the time-dependent Hilbert space [12]. With the two-target time-dependent DMRG procedure, we can cal-

culate time-dependent quantities in Eq. (2) with high accuracy. We keep 6000 density-matrix eigenstates in our tDMRG and use  $M \sim 20$ . In calculating Eq. (2), we truncated time  $s$  up to  $t + 55$  with time increment of 0.02 and performed the integration as a discrete Fourier transform with  $\eta = 0.1$ . In Fig. 7(c), we showed time-resolved dynamical spin correlation function at  $\omega_p = 20$ , where a non-resonant condition gives a very small energy absorption into the system because of  $\omega_p \gg U$ . In such a condition, tDMRG with the 6000 eigenstates provides a reasonable convergence in the spin correlation function. However, if  $\omega_p$  meets a resonance condition with energy absorption, the convergence becomes worse.

In a  $L_x \times L_y$  lattice with open boundary conditions, we define momentum  $\mathbf{q} = (q_x, q_y)$  as  $q_{x(y)} = n_{x(y)}\pi/(L_{x(y)} + 1)$  ( $n_{x(y)} = 1, 2, \dots, L_{x(y)}$ ) and  $S_{\mathbf{q}}^z = 2[(L_x + 1)(L_y + 1)]^{-1/2} \sum_i \sin(q_x i_x) \sin(q_y i_y) S_i^z$ .

- 
- [1] H. Okamoto, T. Miyagoe, K. Kobayashi, H. Uemura, H. Nishioka, H. Matsuzaki, A. Sawa, and Y. Tokura, Photoinduced transition from Mott insulator to metal in the undoped cuprates  $\text{Nd}_2\text{CuO}_4$  and  $\text{La}_2\text{CuO}_4$ , *Phys. Rev. B* **83**, 125102 (2011).
- [2] D. Hsieh, F. Mahmood, D. H. Torchinsky, G. Cao, and N. Gedik, Observation of a metal-to-insulator transition with both Mott-Hubbard and Slater characteristics in  $\text{Sr}_2\text{IrO}_4$  from time-resolved photocarrier dynamics, *Phys. Rev. B* **86**, 035128 (2012).
- [3] X. Li, H. Ning, O. Mehio, H. Zhao, M.-C. Lee, K. Kim, F. Nakamura, Y. Maeno, G. Cao, and D. Hsieh, Keldysh space control of charge dynamics in a strongly driven Mott insulator, *Phys. Rev. Lett.* **128**, 187402 (2022).
- [4] P. Bowlan, S. A. Trugman, X. Wang, Y. M. Dai, S.-W. Cheong, E. D. Bauer, A. J. Taylor, D. A. Yarotski, and R. P. Prasankumar, Directly probing spin dynamics in insulating antiferromagnets using ultrashort terahertz pulses, *Phys. Rev. B* **94**, 184429 (2016).
- [5] G. Batignani, D. Bossini, N. Di Palo, C. Ferrante, E. Pontecorvo, G. Cerullo, A. Kimel, and T. Scopigno, Probing ultrafast photo-induced dynamics of the exchange energy in a Heisenberg antiferromagnet, *Nat. Photonics* **9**, 506 (2015).
- [6] M. P. M. Dean, Y. Cao, X. Liu, S. Wall, D. Zhu, R. Mankowsky, V. Thampy, X. M. Chen, J. G. Vale, D. Casa, J. Kim, A. H. Said, P. Juhas, R. Alonso-Mori, J. M. Glowina, A. Robert, J. Robinson, M. Sikorski, S. Song, M. Kozina, H. Lemke, L. Patthey, S. Owada, T. Katayama, M. Yabashi, Y. Tanaka, T. Togashi, J. Liu, C. Rayan Serrao, B. J. Kim, L. Huber, C.-L. Chang, D. F. McMorrow, M. Först and J. P. Hill, Ultrafast energy- and momentum-resolved dynamics of magnetic correlations in the photo-doped Mott insulator  $\text{Sr}_2\text{IrO}_4$ , *Nat. Mater.* **15**, 601 (2016).
- [7] D. G. Mazzone, D. Meyers, Y. Cao, J. G. Vale, C. D. Dashwood, Y. Shi, A. J. A. James, N. J. Robinson, J. Q. Lin, V. Thampy, Y. Tanaka, A. S. Johnson, H. Miao, R. Wang, T. A. Assefa, J. Kim, D. Casa, R. Mankowsky, D. Zhu, R. Alonso-Mori, S. Song, H. Yavas, T. Katayama, M. Yabashi, Y. Kubota, S. Owada, J. Liu, J. Yang, R. M. Konik, I. K. Robinson, J. P. Hill, D. F. McMorrow, M. Forst, S. Wall, X. Liu, M. P. M. Dean, Laser-induced transient magnons in  $\text{Sr}_3\text{Ir}_2\text{O}_7$  throughout the Brillouin zone, *Proc. Nat. Acad. Sci. USA*, **118**, e2103696118 (2021).
- [8] L. J. P. Ament, M. van Veenendaal, T. P. Devereaux, J. P. Hill, and J. van den Brink, Resonant inelastic x-ray scattering studies of elementary excitations, *Rev. Mod. Phys.* **83**, 705 (2011).
- [9] J.-A. Yang, N. Pellatz, T. Wolf, R. Nandkishore, and D. Reznik, Ultrafast magnetic dynamics in insulating  $\text{YBa}_2\text{Cu}_3\text{O}_{6.1}$  revealed by time resolved two-magnon Raman scattering, *Nat. Commun.* **11**, 2548 (2020).
- [10] A. Secchi, S. Brener, A. I. Lichtenstein, and M. I. Katsnelson, Non-equilibrium magnetic interactions in strongly correlated systems, *Ann. Phys.* **333**, 221 (2013).
- [11] J. H. Mentink, Manipulating magnetism by ultrafast control of the exchange interaction, *J. Phys. Condens. Matter* **23**, 453001 (2017), and references therein.
- [12] K. Shinjo, Y. Tamaki, S. Sota, and T. Tohyama, Density-matrix renormalization group study of optical conductivity of the Mott insulator for two-dimensional clusters, *Phys. Rev. B* **104**, 205123 (2021).
- [13] Y. Wang, T. P. Devereaux, and C.-C. Chen, Theory of time-resolved Raman scattering in correlated systems: Ultrafast engineering of spin dynamics and detection of thermalization, *Phys. Rev. B* **98**, 245106 (2018).
- [14] Y. Wang, Y. Chen, T. P. Devereaux, B. Moritz, and M. Mitrano, X-ray scattering from light-driven spin fluctuations in a doped Mott insulator, *Comm. Phys.* **4**, 212 (2021).
- [15] K. Shinjo and T. Tohyama, Photoinduced absorptions inside the Mott gap in the two-dimensional extended Hubbard model, *Phys. Rev. B* **96**, 195141 (2017).
- [16] K. Tsutsui, K. Shinjo, and T. Tohyama, Antiphase Oscillation in Time-Resolved Spin Structure Factor of a Photoexcited Mott Insulator, *Phys. Rev. Lett.* **126**, 127404 (2021).
- [17] T. Tohyama, Y. Inoue, K. Tsutsui, and S. Maekawa, Exact diagonalization study of optical conductivity in the two-dimensional Hubbard model, *Phys. Rev. B* **72**, 045113 (2005).
- [18] J. Tokimoto, S. Ohmura, and T. Takahashi, private com-

munication.

- [19] T. Shirakawa, S. Miyakoshi, and S. Yunoki, Photoinduced  $\eta$  pairing in the Kondo lattice model, Phys. Rev. B **101** 174307 (2020).

## V. ACKNOWLEDGMENTS

This work was supported by QST President's Strategic Grant(QST Advanced Study Laboratory), by the Japan Society for the Promotion of Science, KAKENHI (Grants No. 19H01829, No. JP19H05825, No. 21H03455, and No. 22K03500) from Ministry of Education, Culture, Sports, Science, and Technology, Japan, and by CREST (Grant No. JPMJCR1661), the Japan Science and Technology Agency, Japan. Part of the computational work was performed using the supercomputing facilities in QST and computational resources of supercomputer FUGAKU provided by the RIKEN Center for Computational Science through the HPCI System Research Project (Project ID: hp210041).

## SUPPLEMENTARY NOTE

In the main text, we showed time-resolved two-magnon Raman (trTMR) spectrum for a half-filled Hubbard model with the nearest-neighbor hopping  $t_h$  and the on-site Coulomb interaction  $U$  given by

$$H_0 = -t_h \sum_{i\delta\sigma} c_{i\sigma}^\dagger c_{i+\delta\sigma} + U \sum_i n_{i\uparrow} n_{i\downarrow}, \quad (\text{S.1})$$

where  $c_{i\sigma}^\dagger$  is the creation operator of an electron with spin  $\sigma$  at site  $i$ , number operator  $n_{i\sigma} = c_{i\sigma}^\dagger c_{i\sigma}$ ,  $i + \delta$  represents four nearest-neighbor sites around site  $i$ . In insulating cuprates such as  $\text{La}_2\text{CuO}_4$ , the second-neighbor hopping  $t'_h$  is necessary for describing its electronic states. Therefore, it is important to investigate the effect of  $t'_h$  on trTMR. The corresponding term is given by  $-t'_h \sum_{i\delta'\sigma} c_{i\sigma}^\dagger c_{i+\delta'\sigma}$ , where  $i + \delta'$  represents four second-neighbor sites around site  $i$ . The Peierls substitution of an external electric field given by a pump pulse is done by  $c_{i,\sigma}^\dagger c_{i+\delta(\delta')\sigma} \rightarrow e^{-i\mathbf{A}(t) \cdot \mathbf{R}_{\delta(\delta')}} c_{i,\sigma}^\dagger c_{i+\delta(\delta')\sigma}$ . Here,  $\mathbf{R}_{\delta(\delta')}$  is the vector from  $i$  to  $i + \delta(\delta')$ , and  $\mathbf{A}(t)$  is the vector potential given by

$$\mathbf{A}(t) = \mathbf{A}_0 e^{-(t-t_0)^2/(2t_d^2)} \cos[\omega_p(t-t_0)], \quad (\text{S.2})$$

where a Gaussian-like envelope centered at  $t_0$  has a temporal width  $t_d$  and a central frequency  $\omega_p$ .

As is the case of the main text, we set  $U = 10$ ,  $t_0 = 0$  and  $t_d = 0.5$  by taking  $t_h = 1$  as an energy unit and  $1/t_h$  as a time unit. In addition, we take  $t'_h = -0.25$  [1]. We then calculate  $B_1$  trTMR spectrum  $M(\omega; t)$  after turning off a pump pulse for a  $4 \times 4$  periodic lattice.  $M(\omega; t)$  was defined in the main text and numerically calculated by using a Lanczos-type exact diagonalization technique. Supplementary Figure 7 shows the  $\omega_p$  dependence of  $M(\omega; t)$  at  $t = 4$ . Similar to the case of  $t'_h = 0$  as shown in Fig. 3 of the main text, the pump pulse suppresses the intensity of the two-magnon peak at  $\omega = 0.95$ , which has been observed in the trTMR experiment for photoirradiated  $\text{YBa}_2\text{Cu}_3\text{O}_{6.1}$  [2]. When  $\omega_p = 6$ , we find an enhancement of low-energy spectral weight around  $\omega = 0.25$ . This is also similar to the case without  $t'_h$  discussed in the main text. These similarities clearly indicate that the presence of  $t'_h$  does not change the emergence of low-energy magnetic excitations caused by photo pumping. We note that a small shift of both the two-magnon peak and photoinduced low-energy structure toward lower energy as compared with the case without  $t'_h$  (see Fig. 3 in the main text) can be attributed to the effect of magnetic frustration induced by second-neighbor superexchange interactions due to finite  $t'_h$ .

In the main text, the polarization vector  $\mathbf{A}_0$  in a pump pulse was set to be along the (1,0) direction, i.e.,

$\mathbf{A}_0 = (A_0, 0)$ . On the contrary, in the trTMR experiment for  $\text{YBa}_2\text{Cu}_3\text{O}_{6.1}$  [2], a polarization vector has been selected to be the (1,1) direction. In order to clarify whether the emergence of photoinduced low-energy

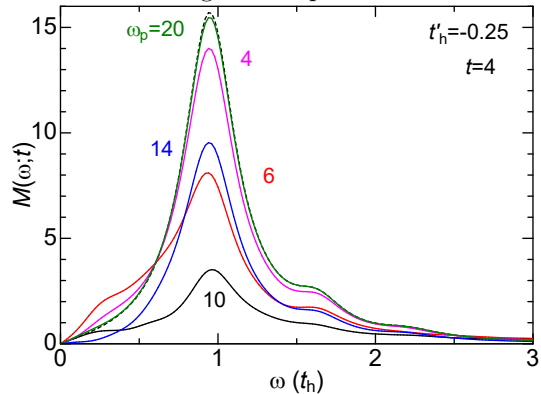


FIG. 7. Pumping frequency  $\omega_p$  dependence of time-resolved two-magnon Raman spectrum  $M(\omega; t)$  at  $t = 4$  after pumping for a half-filled  $4 \times 4$  Hubbard lattice with  $U = 10$  and  $t'_h = -0.25$ . Dashed back line represents the results before pumping, while purple, red, black, blue, and green solid lines represent the results at  $\omega_p = 4, 6, 10, 14,$  and  $20$ , respectively.

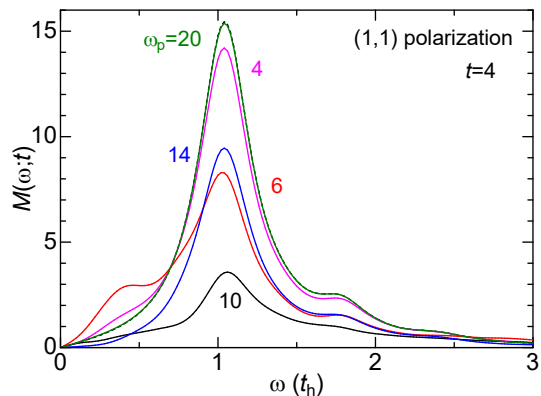


FIG. 8. Pumping frequency  $\omega_p$  dependence of time-resolved two-magnon Raman spectrum  $M(\omega; t)$  at  $t = 4$  after pumping with (1,1) polarization direction for a half-filled  $4 \times 4$  Hubbard lattice with  $U = 10$  and  $t'_h = 0$ . Dashed back line represents the results before pumping, while purple, red, black, blue, and green solid lines represent the results at  $\omega_p = 4, 6, 10, 14,$  and  $20$ , respectively.

magnetic excitations depends on polarization direction or not, we show the  $\omega_p$  dependence of  $B_1$  trTMR spectrum for  $\mathbf{A}_0 = (A_0/\sqrt{2}, A_0/\sqrt{2})$  with  $A_0 = 0.5$  in Supplementary Figure 8. The photoinduced low-energy excitations exist at  $\omega_p = 6$  as is the case of the (1,0) direction. Therefore, we conclude that the low-energy excitations are independent of polarization direction and thus the observed one ranging from  $1000\text{cm}^{-1}$  to  $1500\text{cm}^{-1}$  in  $\text{YBa}_2\text{Cu}_3\text{O}_{6.1}$  can be explained by our interpretation discussed in the main text.

- 
- [1] K. Tsutsui, K. Shinjo, and T. Tohyama, Antiphase Oscillation in Time-Resolved Spin Structure Factor of a Photoexcited Mott Insulator, *Phys. Rev. Lett.* **126**, 127404 (2021).
- [2] J.-A. Yang, N. Pellatz, T. Wolf, R. Nandkishore, and D. Reznik, Ultrafast magnetic dynamics in insulating  $\text{YBa}_2\text{Cu}_3\text{O}_{6.1}$  revealed by time resolved two-magnon Raman scattering, *Nat. Commun.* **11**, 2548 (2020).